Supplementary Information (SI)

Synthesis of micellar-like terpolymer nanoparticles with reductively-cleavable cross-links and evaluation of efficacy in 2D and 3D models of triple negative breast cancer

Patrícia F. Monteiro[a], Muhammad Gulfam[a], Cíntia J. Monteiro[a], Alessandra Travanut[a], Thais Fedatto Abelha[a], Amanda K. Pearce,[a] Christine Jerôme[b], Anna M. Grabowska[c], Philip A. Clarke[c], Hilary M. Collins[a], David M. Heery[a], Pavel Gershkovich[a] and Cameron Alexander[a]*

[a.]School of Pharmacy, University of Nottingham, NG7 2RD, UK. E-mail: cameron.alexander@nottingham.ac.uk; Tel: +44 (0)115 846 7678.

[b.]Cancer Biology, Division of Cancer and Stem Cells, University of Nottingham, NG7 2UH, UK.

[c.]Center for Education and Research on Macromolecules (CERM), University of Liège, Sart-Tilman, B6, 4000 Liège, Belgium.

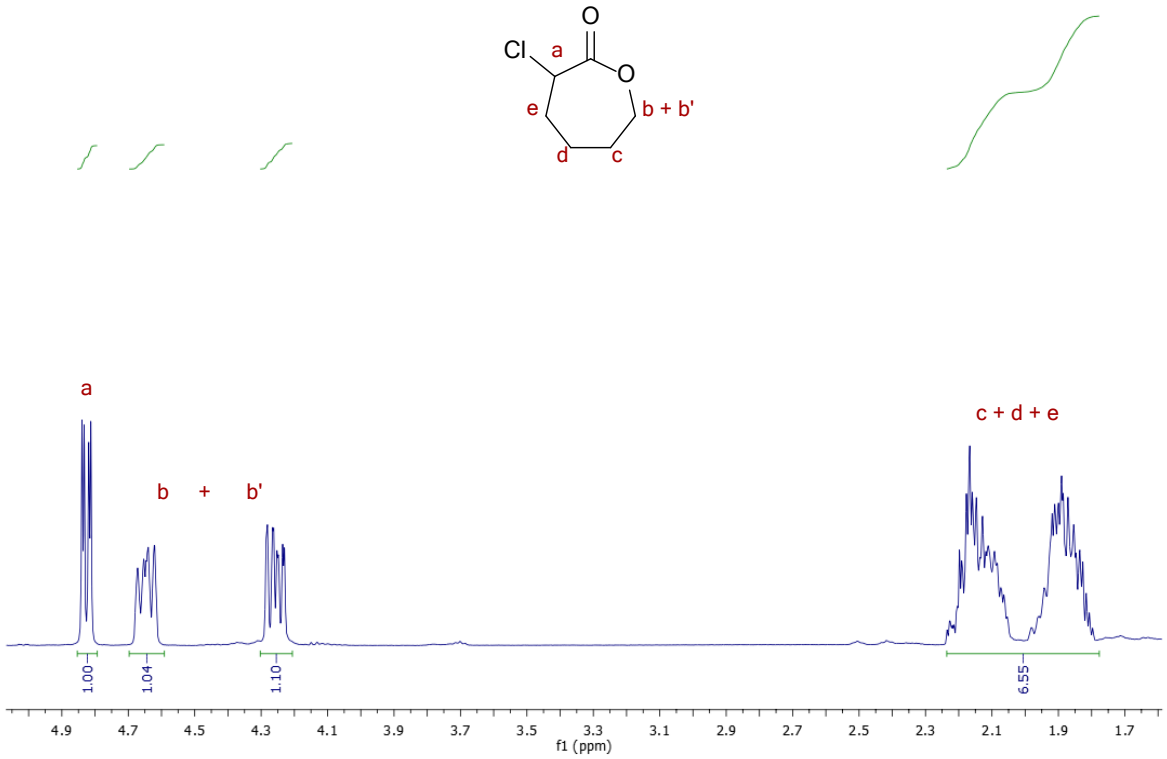

Figure S1 - ^{1}H NMR spectrum of αClεCL in $CDCl_3$.

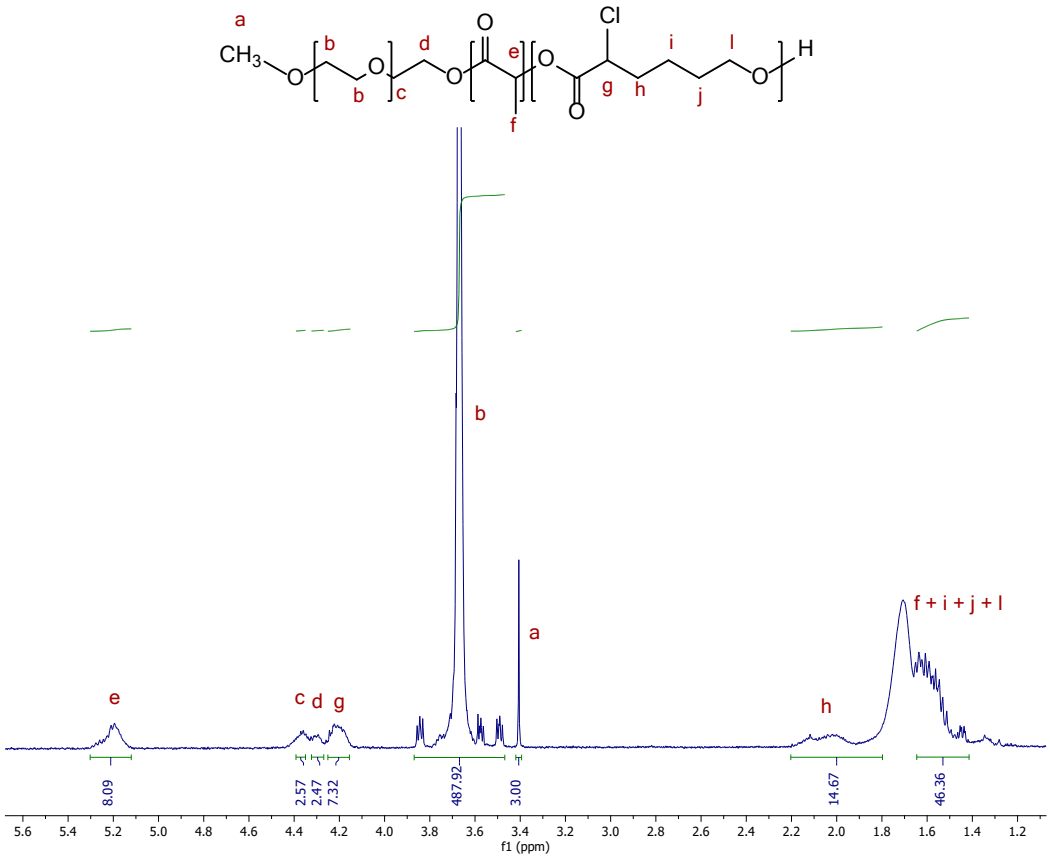

Figure S2 - ^{1}H NMR spectrum of mPEG-*b*-poly(D,L-LA-*co*-α-Cl-ε-CL) in $CDCl_3$.

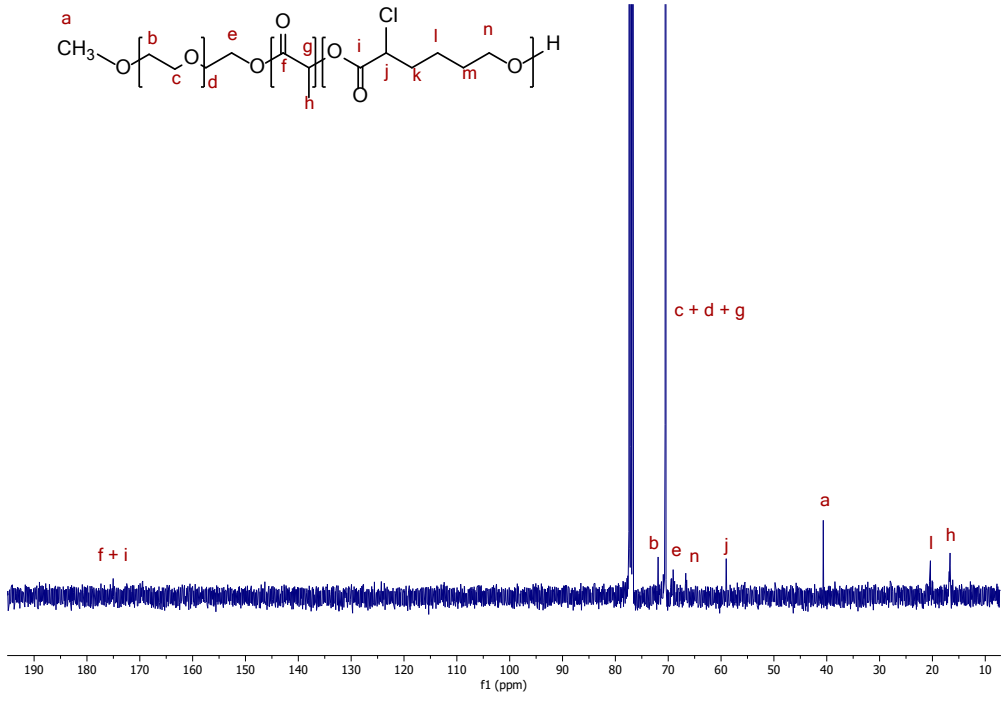

Figure S3 - ^{13}C NMR spectrum of mPEG-*b*-poly(D,L-LA-*co*-α-Cl-ε-CL) in $CDCl_3$.

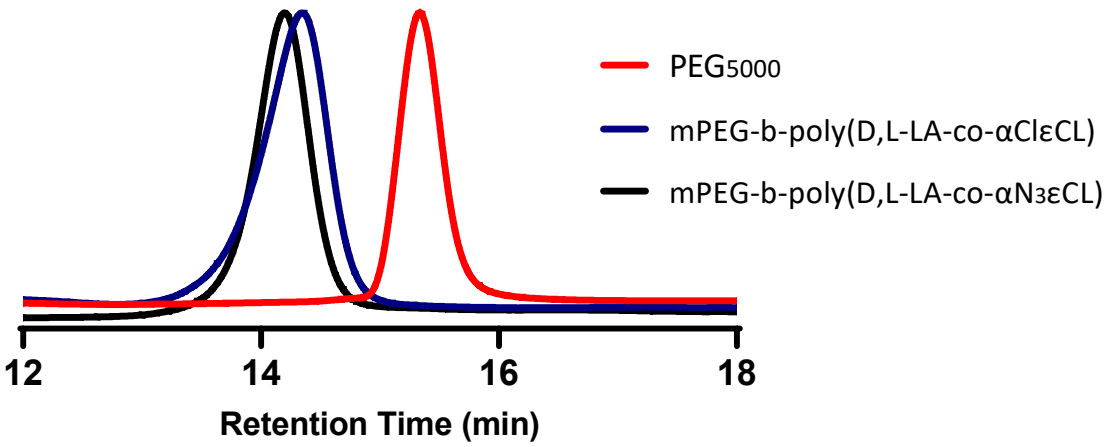

Figure S4 - SEC traces of mPEG-*b*-poly(D,L-LA-*co*-αClεCL), and mPEG-*b*-poly(D,L-LA-*co*-αN_3CL) and $mPEG_{5000}$ in THF.

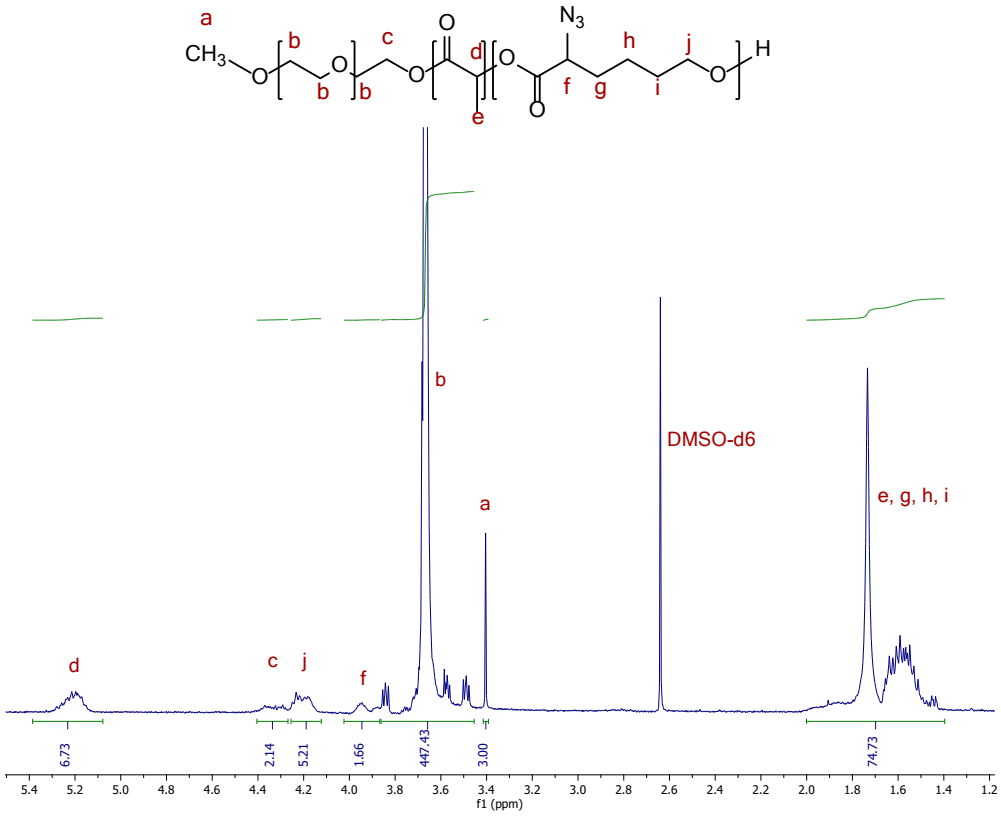

Figure S5 - ^{1}H NMR spectrum of mPEG-*b*-poly(D,L-LA-*co*-α-N_3-ε-CL) in $CDCl_3$.

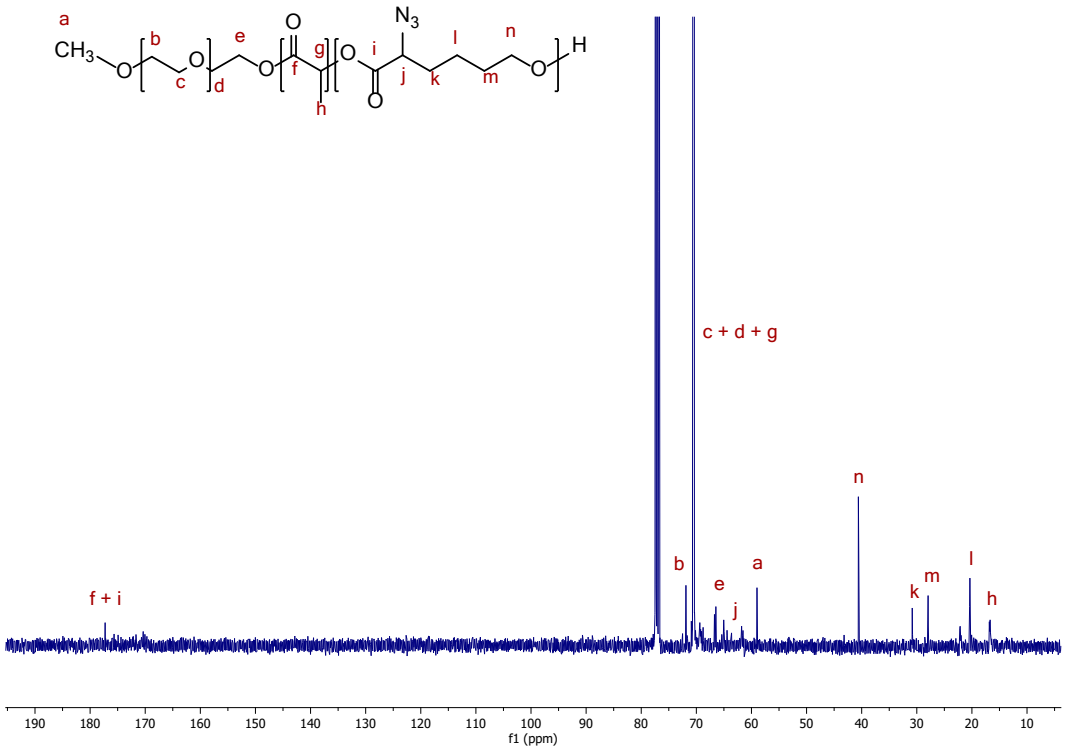

Figure S6 - ^{13}C NMR spectrum of mPEG-*b*-poly(D,L-LA-*co*-α-N_3-ε-CL) in $CDCl_3$.

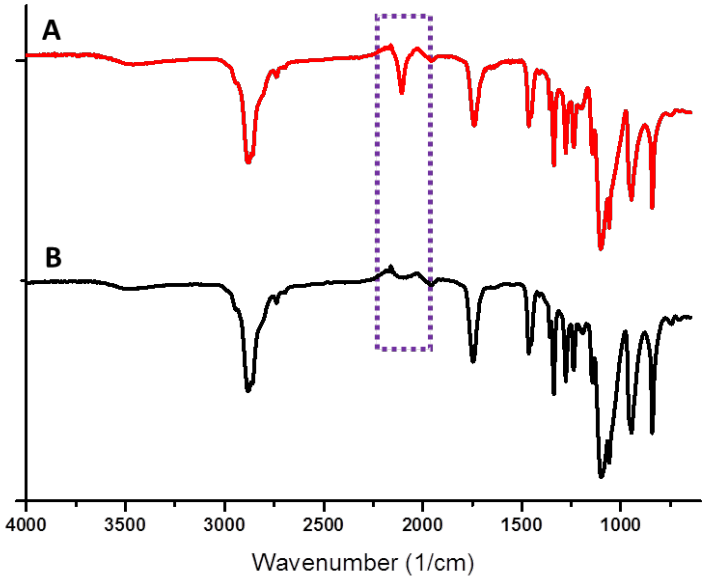

Figure S7 - FT-IR spectra of mPEG-*b*-poly(D,L-LA-*co*-α-N_3-ε-CL) **(A)** and mPEG-*b*-poly(D,L-LA-*co*-α-Cl-ε-CL) **(B)**.

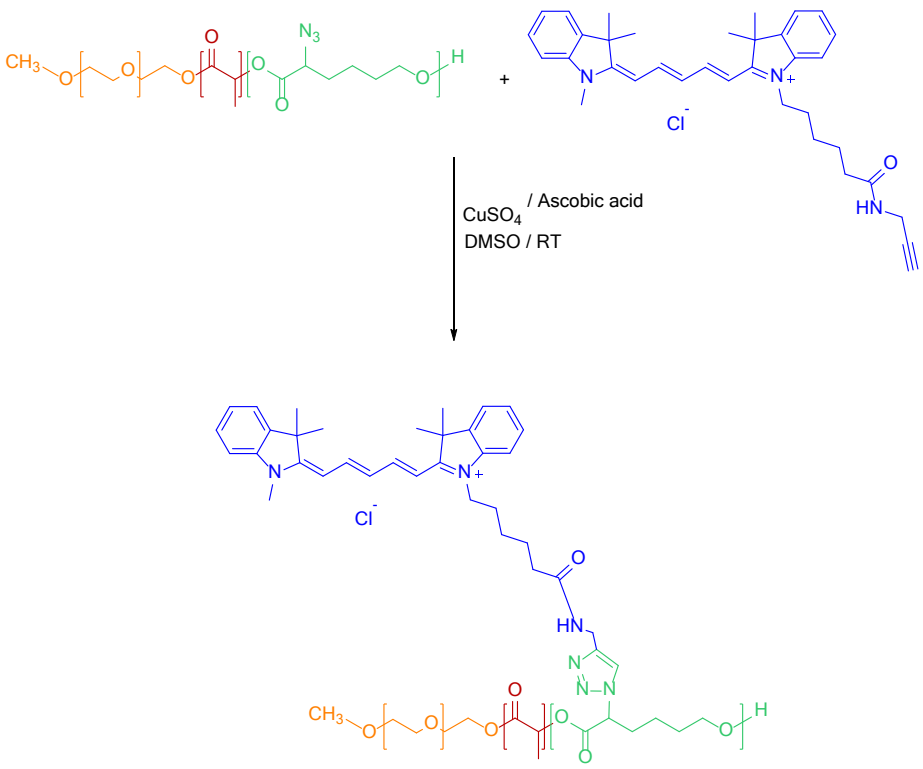

Scheme S1 - Scheme for the synthesis of Cy5 labelled mPEG-*b*-poly(D,L-LA-*co*-α-N_3-ε-CL).

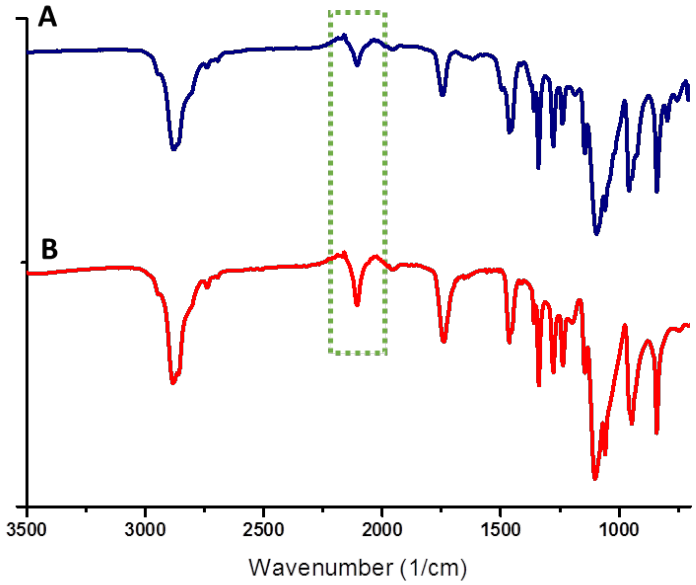

Figure S8 - FT-IR spectra of Cy5-labelled mPEG-*b*-poly(D,L-LA-*co*-α-N_3-ε-CL) **(A)** and unlabelled mPEG-*b*-poly(D,L-LA-*co*-α-N_3-ε-CL) **(B)**.

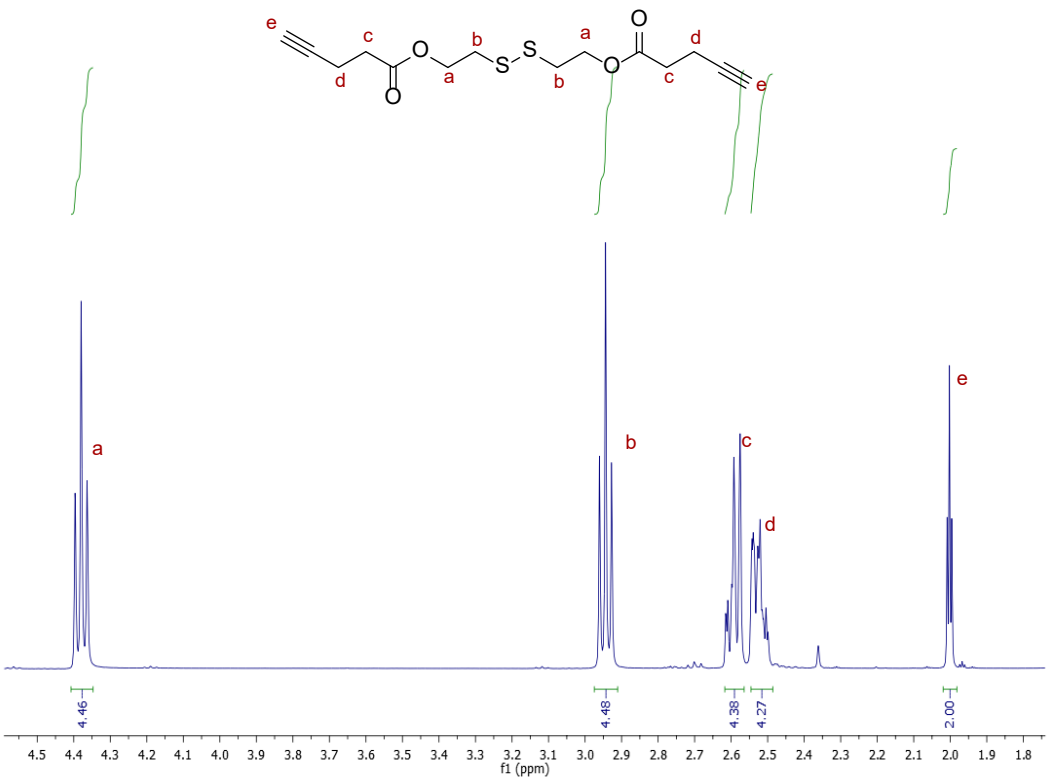

Figure S9 - ^{1}H NMR spectrum of redox-responsive bis-alkyne-ethyl disulfide crosslinker in $CDCl_3$.

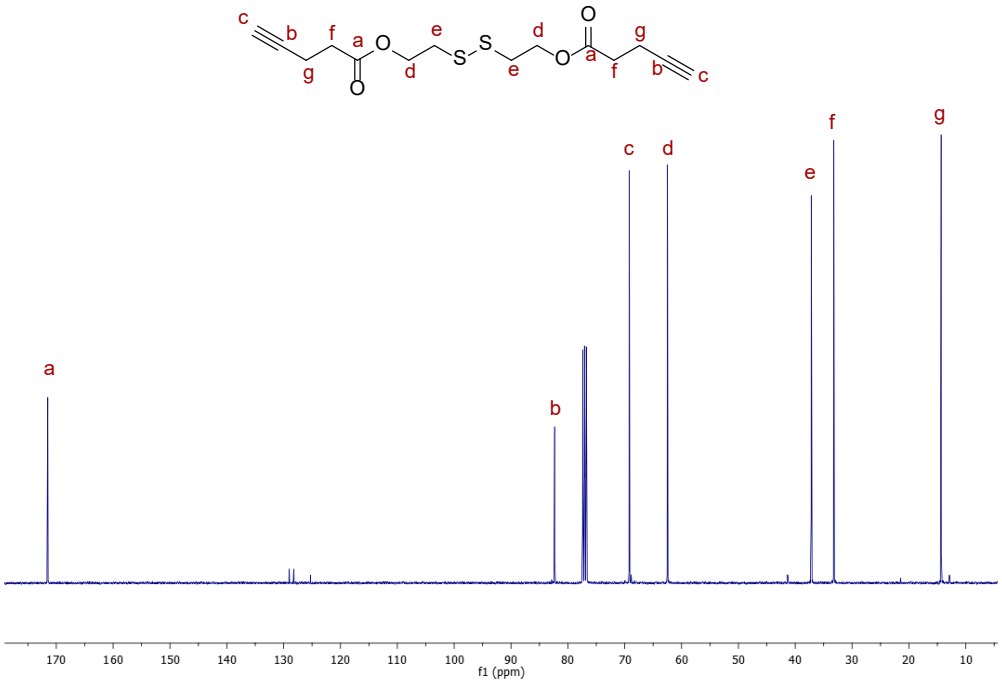

Figure S10 - ^{13}C NMR spectrum of redox-responsive bis-alkyne-ethyl disulfide crosslinker in $CDCl_3$.

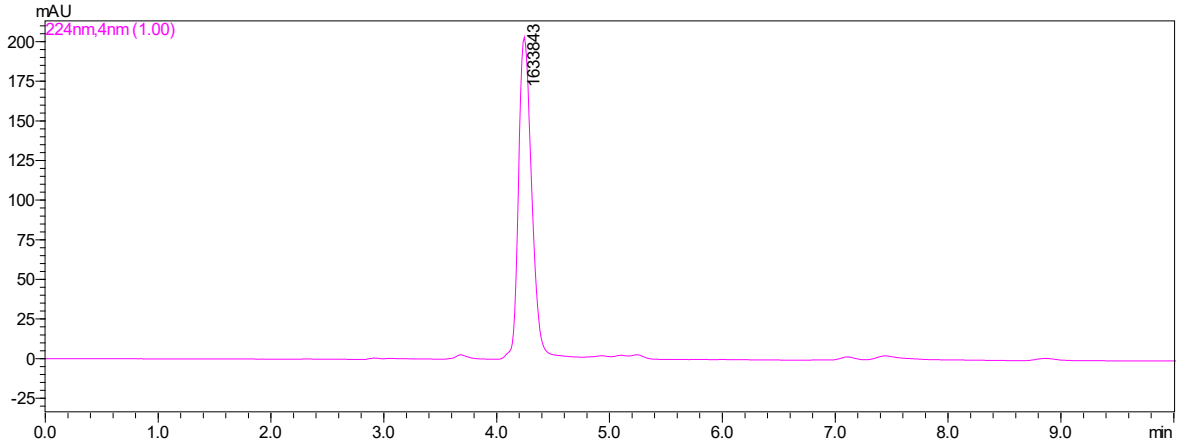

Figure S11 - Chromatogram showing the quantification of docetaxel (DTX) from the DTX-loaded crosslinked micelles using the developed HPLC method.

3D multicellular spheroids of TNBC cells – monoculture

For the FACS analysis, cells were incubated with two different concentrations (50 µg/mL and 150 µg/mL) of MLNPs for 5 h. Figure S12A and B shows the FACS histograms of the cell populations treated with the evaluated concentrations of crosslinked and un-crosslinked MLNPs. Figure S12C indicates the difference in the uptake of Cy5-labelled crosslinked and un-crosslinked MLNPs according to the mean fluorescence intensity (MFI) calculated using Kaluza 1.5 software, and it shows that Cy5-labelled crosslinked MLNPs were internalised to a greater extent than the un-crosslinked MLNPs in 3D spheroids, which corroborates with the assessment of the Cy5-labelled MLNPs in 2D monolayers of the TNBC cells.

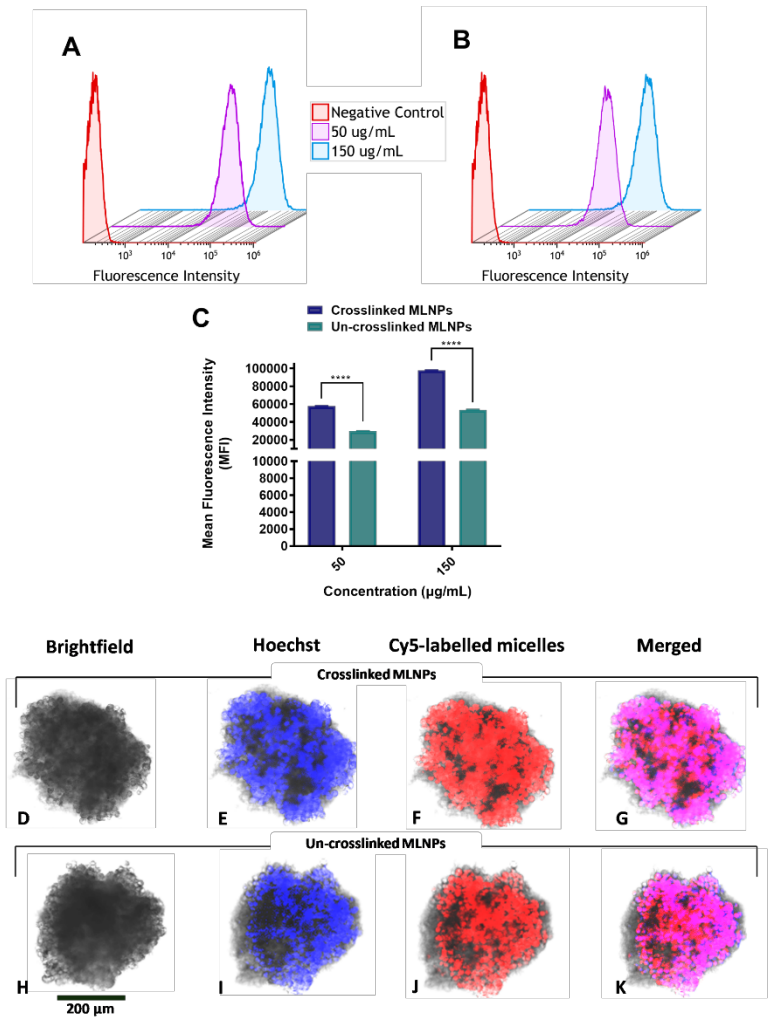

Figure S12 - Uptake of Cy5-labelled crosslinked and un-crosslinked MLNPs in 3D multicellular spheroids of MDA-MB-231 cells. (A,B) FACS uptake histograms for crosslinked (left) and un-crosslinked (right) MLNPs. (C) Quantification of MFI with the concentration of the Cy5-labelled crosslinked and un-crosslinked MLNPs. Data are representative of three experiments (*p < 0.05, **p < 0.01, ****p < 0.0001 two-way ANOVA with Tukey's post-test). Spheroids were allowed to grow for 3 days and then were treated with 50 µg/mL of Cy5-labelled MLNPs for 5 h. Brightfield showing the multicellular spheroids (D, H). Blue channel and brightfield: showing nuclei stained with Hoechst (E, I). Red channel and brightfield: Cy5-labelled crosslinked MLNPs (F) and Cy5-labelled un-crosslinked MLNPs (J). Merged: superimposition of all channels (G, K) – Scale bar 200 µm.

In Figure S12 (D-K) are shown the results of the uptake assessed by confocal microscopy. Spheroid nuclei were stained with Hoechst 33342 dye at a concentration of 1 µg/mL (50 µL)

for 30 minutes. This step for staining the nuclei was optimised by testing different concentrations of Hoechst 33342 dye and incubation time.

3D reconstructions of confocal laser scanning micrographs (zeta-stack) of the spheroids are shown as follows: Brightfield images of the multicellular spheroids are shown in Figure S12 D,H. Nuclei stained with Hoechst 33342 are depicted in Figure S12 E,I, whereas the Cy5-labelled MLNPs within the spheroids are indicated in Figure S12 F,J. Finally, the merged images of the channels are shown in Figure S12 G,K. Zeta-stack images were taken for assessing the penetration ability of the Cy5-labelled MLNPs in 3D spheroids.

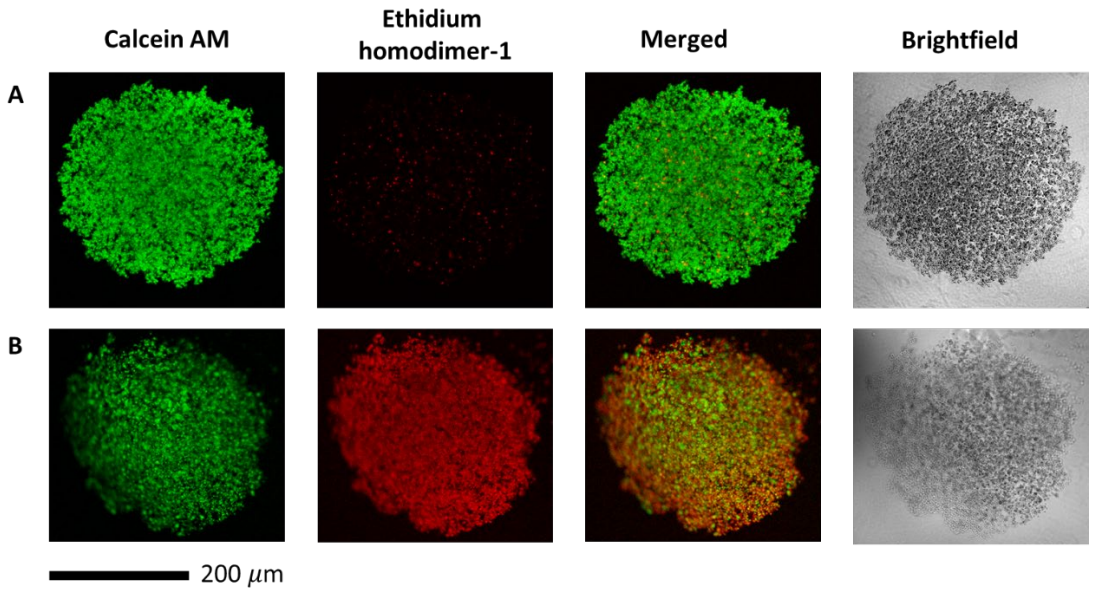

Figure S13 – Controls of the Live/Dead spheroid staining assay using calcein AM and ethidium homodimer-1. Negative control: untreated spheroids (A) and positive control: spheroid treated with 12% of DMSO for 24 h. Both spheroids were subsequently stained with calcein AM and ethidium homodimer-1. Spheroids were imaged using confocal microscopy.

Tukey's multiple comparisons test	Signif	Summary	P Value
Row 1			
Group A vs. Crosslinked Micelles in PBS	No	ns	0.9961
Group A vs. Uncrossinked Micelles in PBS	No	ns	0.9924
Crosslinked Micelles in PBS vs. Uncrossinked Micelles in PBS	No	ns	0.9994
Row 2			
Group A vs. Crosslinked Micelles in PBS	No	ns	0.2683
Group A vs. Uncrossinked Micelles in PBS	No	ns	0.3071
Crosslinked Micelles in PBS vs. Uncrossinked Micelles in PBS	No	ns	0.9961
Row 3			
Group A vs. Crosslinked Micelles in PBS	Yes	*	0.0307
Group A vs. Uncrossinked Micelles in PBS	No	ns	0.0835
Crosslinked Micelles in PBS vs. Uncrossinked Micelles in PBS	No	ns	0.9075
Row 4			
Group A vs. Crosslinked Micelles in PBS	Yes	***	0.0004
Group A vs. Uncrossinked Micelles in PBS	Yes	**	0.0094
Crosslinked Micelles in PBS vs. Uncrossinked Micelles in PBS	No	ns	0.5954
Row 5			
Group A vs. Crosslinked Micelles in PBS	Yes	****	<0.0001
Group A vs. Uncrossinked Micelles in PBS	Yes	**	0.0031
Crosslinked Micelles in PBS vs. Uncrossinked Micelles in PBS	No	ns	0.1462
Row 6			
Group A vs. Crosslinked Micelles in PBS	Yes	****	<0.0001
Group A vs. Uncrossinked Micelles in PBS	Yes	****	<0.0001
Crosslinked Micelles in PBS vs. Uncrossinked Micelles in PBS	Yes	****	<0.0001
Row 7			
Group A vs. Crosslinked Micelles in PBS	Yes	****	<0.0001
Group A vs. Uncrossinked Micelles in PBS	Yes	****	<0.0001
Crosslinked Micelles in PBS vs. Uncrossinked Micelles in PBS	Yes	****	<0.0001
Row 8			
Group A vs. Crosslinked Micelles in PBS	Yes	****	<0.0001
Group A vs. Uncrossinked Micelles in PBS	Yes	****	<0.0001
Crosslinked Micelles in PBS vs. Uncrossinked Micelles in PBS	Yes	****	<0.0001
Row 9			
Group A vs. Crosslinked Micelles in PBS	Yes	****	<0.0001
Group A vs. Uncrossinked Micelles in PBS	Yes	****	<0.0001
Crosslinked Micelles in PBS vs. Uncrossinked Micelles in PBS	Yes	****	<0.0001
Row 10			
Group A vs. Crosslinked Micelles in PBS	Yes	****	<0.0001
Group A vs. Uncrossinked Micelles in PBS	Yes	****	<0.0001
Crosslinked Micelles in PBS vs. Uncrossinked Micelles in PBS	Yes	****	<0.0001
Row 11			
Group A vs. Crosslinked Micelles in PBS	Yes	****	<0.0001
Group A vs. Uncrossinked Micelles in PBS	Yes	****	<0.0001
Crosslinked Micelles in PBS vs. Uncrossinked Micelles in PBS	Yes	****	<0.0001
Row 12			
Group A vs. Crosslinked Micelles in PBS	Yes	****	<0.0001
Group A vs. Uncrossinked Micelles in PBS	Yes	****	<0.0001
Crosslinked Micelles in PBS vs. Uncrossinked Micelles in PBS	Yes	****	<0.0001
Row 13			
Group A vs. Crosslinked Micelles in PBS	Yes	****	<0.0001
Group A vs. Uncrossinked Micelles in PBS	Yes	****	<0.0001
Crosslinked Micelles in PBS vs. Uncrossinked Micelles in PBS	Yes	****	<0.0001

Figure S14 – Statistical analysis of docetaxel (DTX) release from DTX-loaded crosslinked MLNPs with and without 10 mM of GSH, to mimic a redox and non-redox environment, and DTX-loaded un-crosslinked MLNPs. (*$p < 0.05$, **$p < 0.01$, two-way ANOVA with Tukey's post-test).

Synthesis of hexane-1,6-diyl bis(pent-4-ynoate)

Hexane-1,6-diyl bis(pent-4-ynoate) was synthesised by dissolving 4-pentynoic acid (0.92 g, 9.3 mmol) into a flask containing 40 mL of anhydrous N,N-dimethylformamide. Afterwards, N,N-diisopropylethylamine (1.20 g, 9.30 mmol) was added under stirring followed by HATU (3.58 g, 9.3 mmol). The reaction was left stirring at room temperature for 15 min and finally 1,6-hexanediol (0.5 g, 4.23 mmol) was added and the reaction was left running for 48 h at room temperature. The purification of the crude product was carried out by column chromatography (hexane: ethyl acetate 9:1) yielding 0.14 g, (12%). ^{1}H NMR (400 MHz, $CDCl_3$) δ 4.07 – 4.07 (m, 4H), 2.50-2.45 (m, 8H), 1.95 - 1.93 (m, 2H), 1.62 - 1.59 (m, 4H), 1.37 – 1.33 (m, 4H).

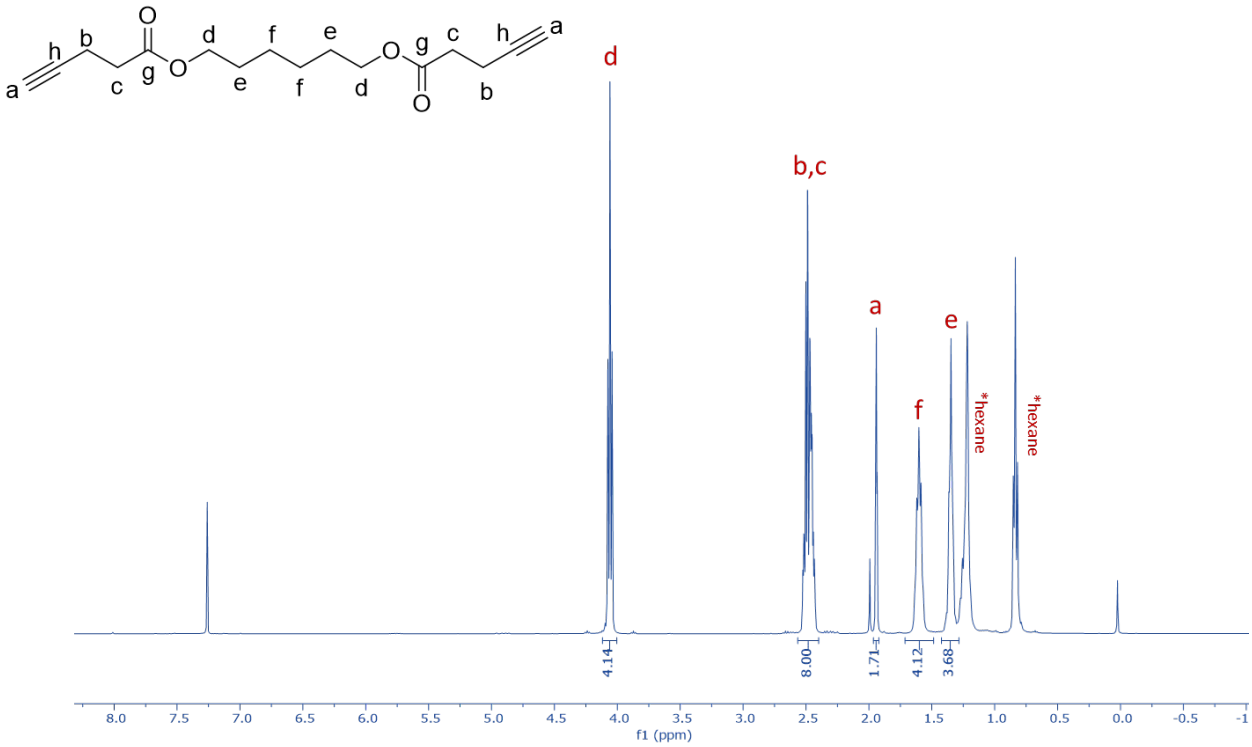

Figure S15 - ^{1}H NMR spectrum of hexane-1,6-diyl bis(pent-4-ynoate) in $CDCl_3$.

Synthesis of mPEG-b-poly(εCL-co-αClεCL)

The copolymer was synthesised by ROP (ring-opening polymerisation) of α-chloro-ε-caprolactone and ε-caprolactone using $mPEG_{5000}$ as a macroinitiator and $Sn(Oct)_2$ (tin-(2-ethylhexanoate)) as a catalyst. ε-CL (0.4 g) and chloro-ε-caprolactone (0.104 g) were transferred into a flask containing $mPEG_{5000}$ (0.5 g) which was previously dried by azeotropic distillation with anhydrous toluene. The contents were heated at 90ºC and solubilized with 10 mL of anhydrous toluene added into the sealed flask under nitrogen atmosphere. At this moment, $Sn(Oct)_2$ (14 mg) was added and the reaction was left to proceed at 90ºC for 24 h under stirring. Afterwards, the reaction was cooled to room temperature. The product was dissolved in dichloromethane and precipitated in diethyl ether. It was then filtered and dried under reduced pressure until constant weight was achieved. ^1H NMR (400 MHz, $CDCl_3$) δ (ppm): 4.35 (CH_2–O–CO, t, 2H), 4.27 (CO–CH(Cl)–CH_2–CH_2–CH_2–CH_2–O–, t, 7H), 4.21 (CO–CH(Cl)–CH_2–CH_2–CH_2–CH_2–O–, t, 14H), 4.08 (CO–CH_2–CH_2–CH_2–CH_2–CH_2–O–H, t, 70H), 3.66 (O–CH_2–CH_2–O–, m, 586H), 3.40 (CH_3–O–, s, 3H), 2.33 (CO–CH_2–CH_2–CH_2–CH_2–O–H, t, 70H), 2.0 (CO–CH(Cl)–CH_2–CH_2–CH_2–CH_2–O–, m, 28H), 1.76–1.32 (CO–CH_2–CH_2–CH_2–CH_2–CH_2–O– and, CO–CH(Cl)–CH_2–CH_2–CH_2–CH_2–O–, m, 248H).

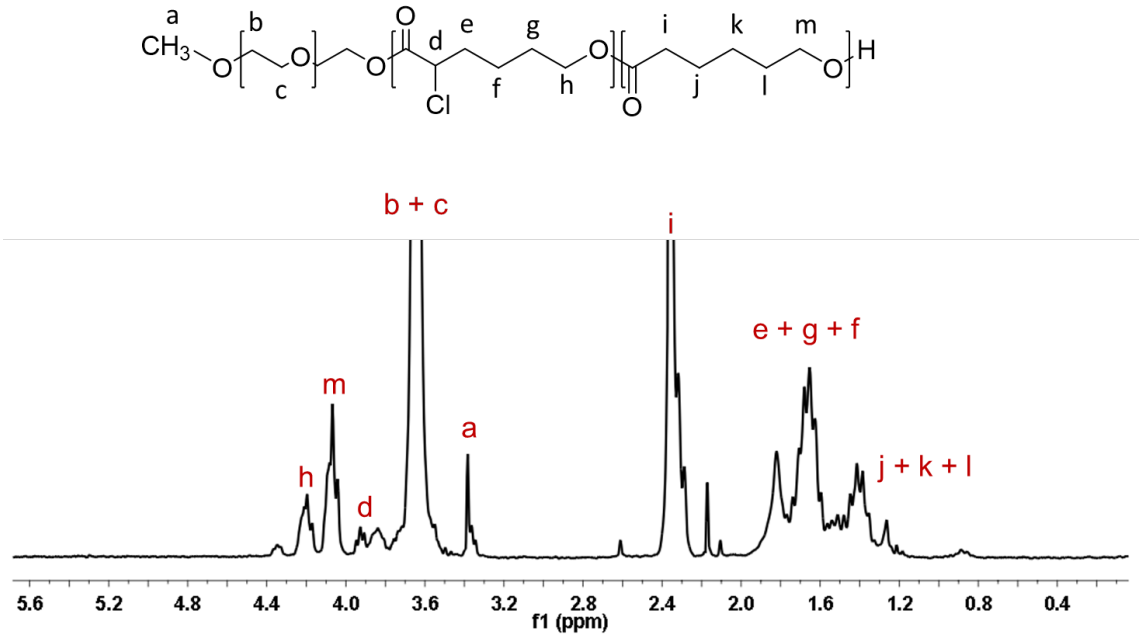

Figure S16 - ^1H NMR spectrum of mPEG-b-poly(εCL-co-αClεCL) in $CDCl_3$.

Synthesis of mPEG-b-poly(εCL-co-αN$_3$εCL)

The azide-functionalised copolymer was obtained through a substitution reaction between chloro and azide groups. Typically, mPEG-*b*-poly(εCL-*co*-α-Cl-ε-caprolactone) (0.50 g) was transferred into a flask and dissolved in 3 mL of DMSO (dimethyl sulfoxide). Subsequently, sodium azide (34 mg) was carefully added and the reaction was allowed to proceed for 24 h at room temperature. The product was dissolved in a small amount of dichloromethane and extracted with diethyl ether to remove DMSO before filtering. The reaction product was then dissolved in toluene and centrifuged in order to remove the insoluble salts followed by the precipitation of the polymer in diethyl ether. The obtained functionalised copolymer was filtered and dried under reduced pressure until constant weight was achieved. ^{1}H NMR (400 MHz, $CDCl_3$) δ (ppm): 4.35 (CH_2–O–CO, t, 2H), 4.23 (CO–CH(N_3)–CH_2–CH_2–CH_2–CH_2–O–, t, 14H), 4.08 (CO–CH_2–CH_2–CH_2–CH_2–CH_2–O–H, t, 70H), 3.89 (CO–CH(N_3)–CH_2–CH_2–CH_2–CH_2–O–, t, 7H), 3.66 (O–CH_2–CH_2–O–, m, 586H), 3.40 (CH_3–O–, s, 3H), 2.33 (CO–CH_2–CH_2–CH_2–CH_2–CH_2–O–H, t, 70H), 1.93–1.34 (CO–CH(N_3)–CH_2–CH_2–CH_2–CH_2–O–, and, CO–CH_2–CH_2–CH_2–CH_2–CH_2–O–H, m, 266H).

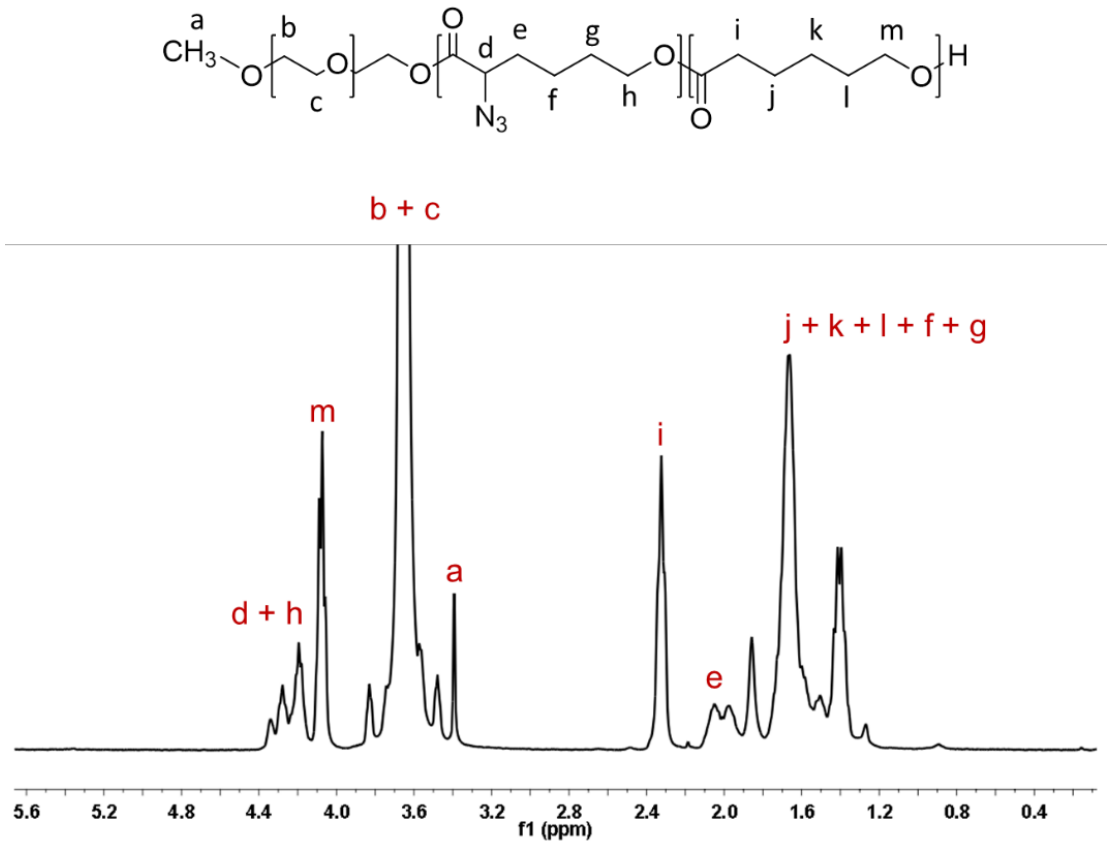

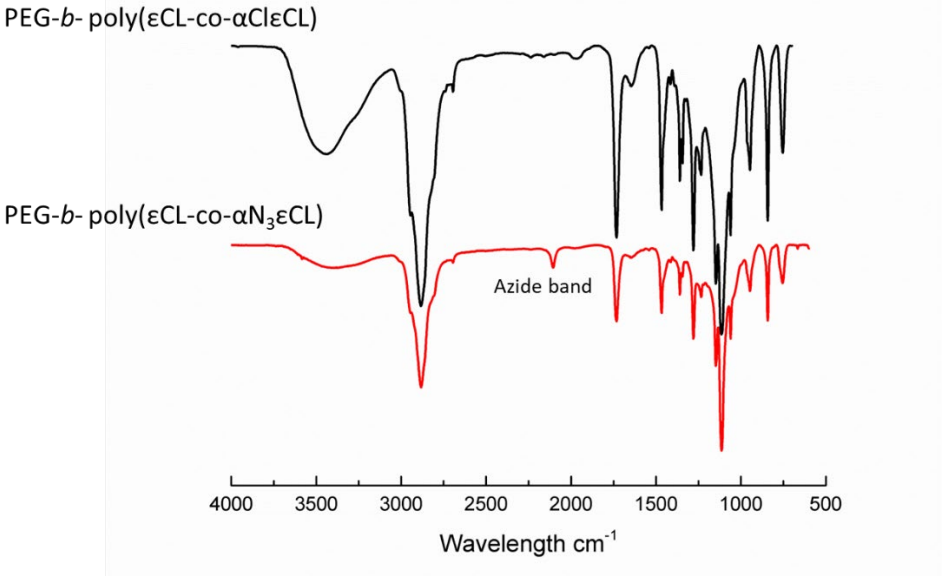

Figure S17 - ^{1}H NMR spectrum of mPEG-*b*-poly(εCL-*co*-αN_3εCL) in $CDCl_3$ and FT-IR spectra of mPEG-*b*-poly(CL-*co*-α-Cl-ε-CL) and mPEG-*b*-poly(CL-*co*-α-N_3-ε-CL).

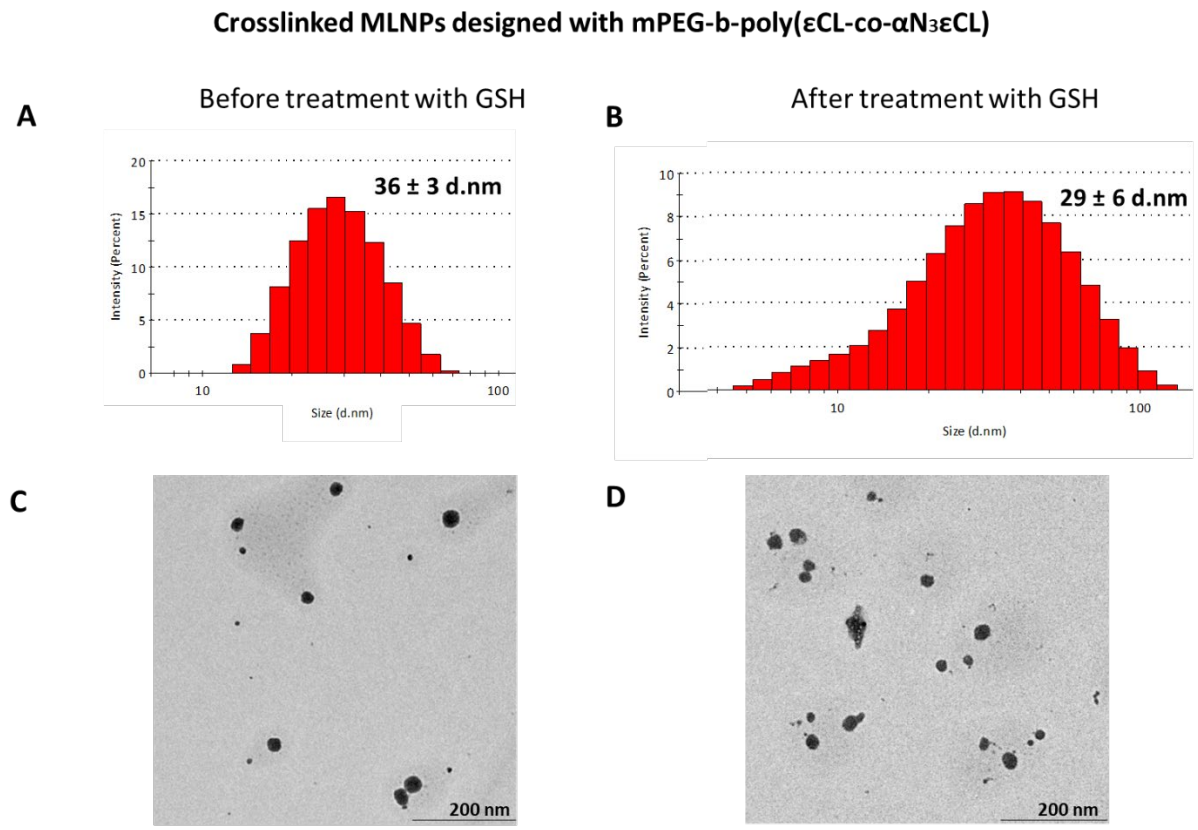

Figure S18 - (A) Size distribution (DLS) of empty redox responsive crosslinked MLNPs prepared using mPEG-*b*-poly(εCL-co-αN$_3$εCL) and (B) DLS of the redox responsive crosslinked MLNPs after the treatment with glutathione (GSH) 10 mM for 3 hours. Size was based on intensity measured by DLS (n=3). (C) Morphology of the crosslinked MLNPs before and (D) after treatment with GSH by transmission electron microscopy.

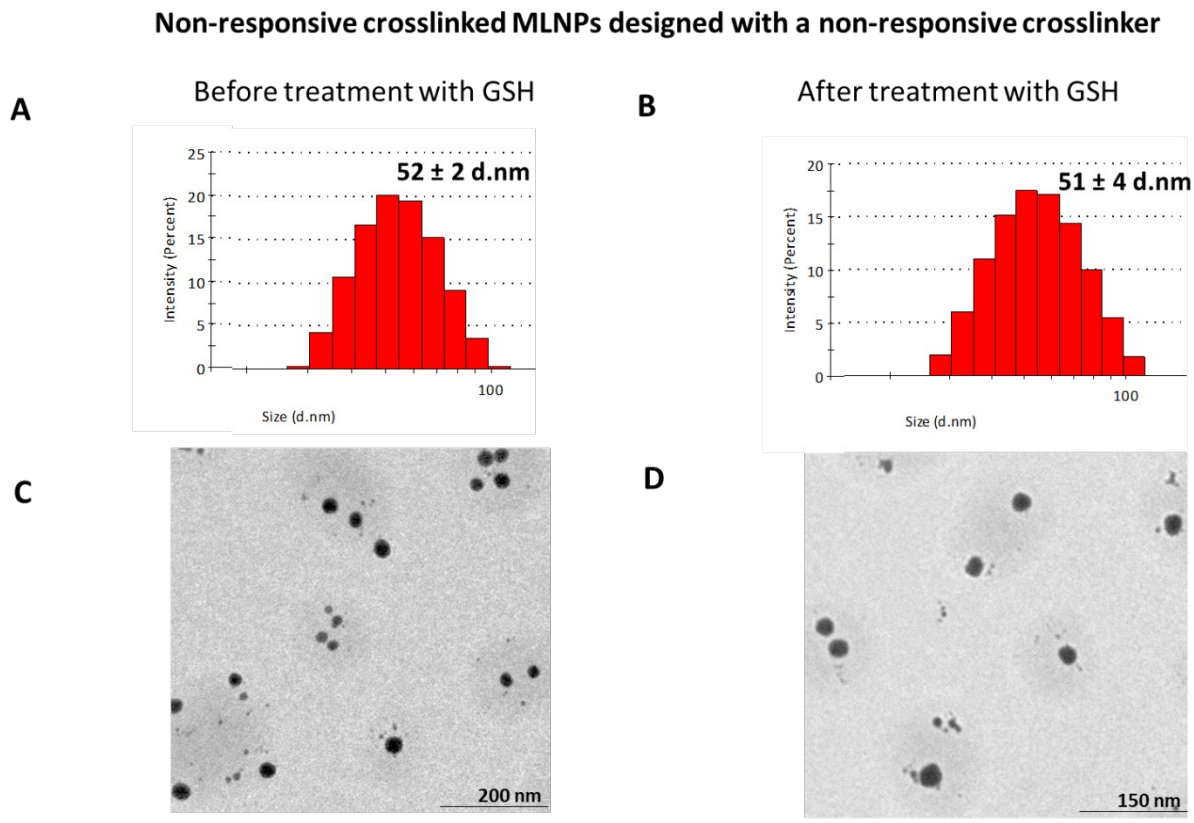

Figure S19 - (A) Size distribution (DLS) of empty non-responsive crosslinked MLNPs prepared using mPEG-*b*-poly(LA-*co*-αN$_3$εCL) and (B) DLS of the non-responsive crosslinked MLNPs after the treatment with glutathione (GSH) 10 mM for 3 hours. Size was based on intensity measured by DLS (n=3). (C) Morphology of the non-responsive crosslinked MLNPs before and (D) after treatment with GSH by transmission electron microscopy.

Assessment of intracellular GSH using GSH-Glo™ Glutathione Assay

The evaluation of intracellular GSH in MDA-MB-231, MCF7, and MCF10A was performed using the GSH-Glo™ Glutathione Assay, Promega. Briefly, MDA-MB-231, MCF7, and MCF10A cells were seeded into a 96 well-plate at a density of 5×10^3 cells per well and incubated at 37°C and 5% of CO_2 for 24 h. Afterwards, the medium was carefully removed from the wells and 100µl of prepared 1X GSH-Glo™ Reagent was added to each well. Plates were mixed briefly on a plate shaker and then incubated for 30 min. 100µl of reconstituted Luciferin Detection Reagent was added to each well and again, the plates were mixed briefly. Finally, plates were incubated for 15 min and the luminescence was measured.